Robotica: (2020) volume 38, pp. 1359–1380. © Cambridge University Press 2019
doi:10.1017/S0263574719001516

A New Gantry-Tau-Based Mechanism Using Spherical Wrist and Model Predictive Control-Based Motion Cueing Algorithm

Mohammad Reza Chalak Qazani*, Houshyar Asadi and Saeid Nahavandi

Institute for Intelligent Systems Research and Innovation, Deakin University, Waurn Ponds Campus, Geelong, Victoria 3217, Australia.
E-mails: houshyar.asadi@deakin.edu.au, saeid.nahavandi@deakin.edu.au

(Accepted October 5, 2019. First published online: October 31, 2019)

SUMMARY
The 3 degree-of-freedom Gantry-Tau manipulator with the addition of the spherical wrist mechanism which is called Gantry-Tau-3R is designed as a high-G simulation-based motion platform (SBMP) with the capability of generating the large linear and angular displacement. The combination of both parallel and serial manipulator in newly designed Gantry-Tau-3R mechanism improves the ability of the mechanism to regenerate larger motion signals with higher linear acceleration and angular velocity. The high-frequency signals are reproduced using the parallel part of the mechanism, and sustainable low-frequency accelerations are regenerated via the serial part due to the larger rotational motion capability, which will be used through motion cueing algorithm tilt coordination channel. The proportional integral derivative (PID) and fuzzy incremental controller (FIC) are developed for the proposed mechanism to show the high path tracking performance as a motion platform. FIC reduces the motion tracking error of the newly designed Gantry-Tau-3R and increases the motion fidelity for the users of the proposed SBMP. The proposed method is implemented using Matlab/Simulink software. Finally, the results demonstrate the accurate motion signal generation using linear model predictive motion cues with a fuzzy controller, which is not possible using the common parallel and serial manipulators.

KEYWORDS: Simulation-based motion platform; High-G Gantry-Tau-3R manipulator; PID controller; FIC; Linear Model Predictive-based Motion Cueing Algorithm.

1. Introduction

The simulation-based motion platforms (SBMPs) are useful research devices to study road safety, test the newly designed vehicles and train vehicle users. Reduction of the costs, time and damages makes SBMP a popular device in research laboratories.[1]

Haward[2] developed the first flight trainer device in 1930. The equipment used the force of the wind to response to the pilots' behaviours. However, it was not able to work in the absence of wind. Edwin Link is the founder of the first electro-mechanic vehicle SBMP.[3] The first commercial SBMP was manufactured for Pan American Airways in 1947.[4] However, it was not able to move and had no visual system. The practical optical systems were not designed until the 1990s.[5] SBMPs were not seriously used until the late 1950s due to the difficulty in generating motion cues. The introduction

* Corresponding author. E-mail: m.r.chalakqazani@gmail.com

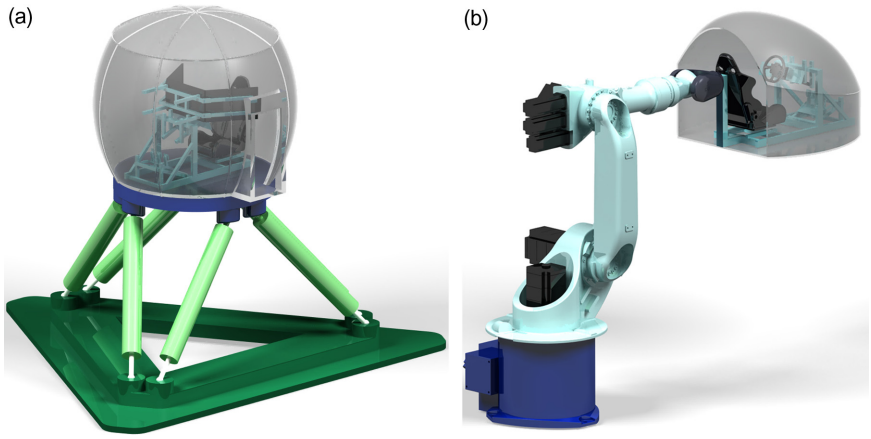

Fig. 1. The structure of (a) parallel manipulator (b) serial manipulator.

of the 6 degree-of-freedom (6-DoF) Stewart-Gough platform led to motion cues by regenerating the longitudinal, lateral and vertical accelerations as well as roll, pitch and yaw velocities. The first driving SBMP with 3-DoF was manufactured by Volkswagen in the early 1970s.[6] In following years, the automotive industries such as IFAS, VTI, FORD, BMW, WIVW, Renault, Nissan, Toyota, etc.[7,8] used the 6-, 7- and 8-DoF SBMPs for all kinds of vehicles throughout the 1990s. The innovation of the Famulus[9] as a first serial manipulator with 6-DoF in 1973 was taken into consideration because of a larger angular displacement during different manoeuvres[10] due to the open-loop structure of this mechanism. It was used as a flight SBMP by Teufel et al.[11] for the first time. It found its way rapidly because of the tremendous beneficial advantages in the research laboratories such as European Centre for Research on Human Movement (EuroMov) and Institute for Intelligent Systems Research and Innovation (IISRI) at Deakin University.

According to their structures, the SBMPs can be divided into two groups, namely, parallel and serial as shown in Fig. 1(a) and (b). The parallel or close-loop manipulators consist of closed kinematic chains, while the serial or open-loop manipulators are connected like a chain to make a desired motion to the end effector. These structures have their advantages and disadvantages. The parallel-based manipulators are widely used as SBMPs for driving because of high stiffness, large payload and high speed and acceleration capacities.[12,13] On the other hand, the parallel manipulators' angular displacement is limited because of the passive joints inside the closed form structures.[14,15] The parallel manipulators consist of several passive joints which are connected to each other in the close chain connection between the base and the end effector.[16–18] The end effector of the manipulator can reach the angular positioning limits if one of the passive joints passes the limitations without consideration of the other passive joints.[19] Nevertheless, the control of parallel manipulators is more straightforward compared with serial manipulators due to their analytical inverse kinematics. These motion simulation platforms are more suitable for driving simulations when there is no need for large rotations. On the other hand, the serial manipulators have a large angular displacement compared with parallel manipulators due to the absence of passive joints in their structure. Then they are more appropriate to be used for flight simulation when larger angular displacements at the end effector are required. However, the control of them is not as easy as a parallel manipulator because they always do not have analytical inverse kinematics. In addition, the consideration of nonlinear constraints of serial manipulators, higher risk of reaching to linear workspace limitations, singular points and isometric configurations with the different arrangement of inputs are the other disadvantages of the serial mechanisms. These limitations of the serial manipulator are open gaps for the researchers in control and mechanical domains.

The first 3-DoF parallel Gantry-Tau which is shown in Fig. 2 is introduced by Johannsson et al.[20] The first Gantry-Tau prototype was built at the University of Queensland, in 2004,[21] and Williams et al.[22] introduced the early version of the Gantry-Tau mechanism with 3-DOF. The triangle arm and the end effector platform were designed to maximise the workspace area of the mechanism.[23] Dressler et al. have investigated the accuracy of the kinematic and dynamic models of the Gantry-Tau mechanism.[24]

https://doi.org/10.1017/S0263574719001516 Published online by Cambridge University Press

Fig. 2. 3-Degree-of-freedom (DoF) Gantry-Tau mechanism.[24]

The two main strategies for the control scheme of the parallel manipulators are error based and model based.[25] The error-based controller is based on the joint space of the model by measuring the active joint positions of the manipulator. The classical PID controller which is tremendously used in industries is an error-based controller. Despite the simplicity, cost-effective and practicality of the proportional integral derivative (PID) controller, it is not a suitable choice for a parallel manipulator.[26] They are not able to guarantee parallel manipulators' high performance because of the nonlinearity of the parallel structures. The fuzzy incremental controller (FIC) has been used in industries with some success.[27] The application of fuzzy PID controllers has been investigated by researchers in recent years[28–32] because of its capability to follow the motion signals with high frequencies.

The proposed manipulator, which is studied in this paper for a high-G SBMP, is called Gantry-Tau-3R. Unlike the parallel manipulator, the Gantry-Tau-3R has a high capability of the angular displacement because of the serial spherical wrist mechanism. It also benefits the large linear displacement because of the Gantry-Tau unique structure.[24] It turns the Gantry-Tau-3R into a high-potential high-G SBMP using the linear model predictive control (MPC) and the motion cueing algorithm (MCA). The regeneration of the motion signals according to the limited workspace boundaries of the SBMP to make the realistic motion feeling is the task of MCA.[33–35] The idea of using MPC for regenerating the accurate MCA known as MPC-based MCA is introduced by Dagdelen et al.[36] However, their developed model[36] quickly reaches the workspace limitations of the SBMP due to the lack of tilt coordination channel consideration. The tilt coordination channel uses the advantage of human vestibular model to reproduce the sustainable acceleration known as somatogravic illusion.[37] Garrett and Best[38] considered the physical limitations of the Hexapod SBMP (pods' lengths) to regenerate the more accurate motion signal. They[38] used the linearised inverse kinematic model of the hexapod in state space model of the MPC. Mohammadi et al.[39,40] introduced the new inhomogeneous weighting and an NN technique to enhance the efficiency of the MPC and predict future reference, respectively. Mohammadi et al.[41] used the single-objective genetic algorithm (GA) to find the optimal MPC horizons for reducing the computational burden of the hardware and increasing the efficiency of the system. Also, they[42] used the multiobjective GA to extract the optimal tuning weights of the MPC model. Qazani et al.[43] proposed the MPC with consideration of the human vestibular model including semicircular system and otolith organs as two specific mathematical model to control the tilt coordination channel separately. Their algorithm[43] is suitable for an SBMP with high restricted workspace boundaries. Later, Qazani et al.[44] considered the inverse kinematics model of the SBMP to attain the more realistic motion signal compared to the existing models.

The regeneration of large motion signals with high linear acceleration (above 5 m/s^2) and angular velocity are not possible via purely parallel or serial manipulators due to the workspace limitations. In this study, the 6-DoF Gantry-Tau-3R is modelled and implemented for the first time with PID and FIC to track the motion signals of the MPC-based MCA as a high-G SBMP. The combination of both parallel and serial manipulators has helped to regenerate the motion signals with larger linear and angular displacements because of the parallel and serial parts of the mechanism, respectively. In addition, the

https://doi.org/10.1017/S0263574719001516 Published online by Cambridge University Press

FIC is designed for the Gantry-Tau-3R mechanism to reduce the motion tracking error of the mechanism which in turn increases the motion fidelity for the SBMP users. The main difference between the newly designed mechanism and traditional Stewart platform is the capability of the Gantry-Tau-3R in regenerating higher high-frequency signal as well as more sustainable low-frequency signal due to the larger angular displacement. The main difference between the newly designed mechanism and traditional Stewart platform is the capability of the Gantry-Tau-3R in regenerating higher high-frequency signal as well as more sustainable low-frequency signal due to higher angular displacement. The mechanism is designed using CAD software and imported in SimMechanic environment of MATLAB software to show the beneficial point of the mechanism via the FIC. The quantitative study has been conducted to prove the effectiveness of the proposed method, while the mathematical model of human vestibular system is incorporated to monitor the motion sensation error. It should be noted that the main phase for developing this mechanism, that is, the controller and MCA, is the quantitative phase followed by a comprehensive testing procedure for all driving scenarios to ensure safety, minimise tracking error and maximise motion realism.

The FIC reduces the motion tracking error to improve the motion fidelity and prevent the motion sickness caused by the discrepancy between the visually perceived movement and the vestibular system's sense of movement.

The Gantry-Tau-3R mechanism and kinematics are explained in Section 2. In Section 3, the PID and FIC of the mechanism are modelled and implemented. The PID and FIC gains are tuned using GA. The MPC-based MCA is modelled and implemented in Section 4. The extracted PID and FIC have been modelled in MATLAB/Simulink software, with consideration of the MPC-based MCA in Section 5. The results are provided and discussed for the proposed SBMP in Section 6. The concluding remarks are presented in Section 7.

2. Gantry-Tau-3R-Based SBMPs

2.1. Gantry-Tau-3R mechanism

The Gantry-Tau-3R manipulator is a 6-DoF parallel kinematic manipulator. This mechanism consists of three active prismatic joints, three active revolute joints and six passive links connecting the prismatic active joints to the platform that shape three sets of arms. The three arms are connected to the prismatic joints through a cart mechanism. Other three arms connect the platform to the cockpit through three active revolute joints.

Figure 3(a) shows the schematic model of the recently proposed Gantry-Tau-3R mechanism. As shown in the schematic model of the Gantry-Tau mechanism in Fig. 3(a), arms 1, 2 and 3, respectively, consist of 1, 2 and 3 links that connect the carts and the platform. Also, arms 4, 5 and 6 are used to implement the yaw, pitch and roll angular displacement of the cockpit.

The simple mechanism of the passive links allows flexibility in the geometric design of the linkages and leads to low manufacturing costs for these manipulators. The universal joints' offsets on the actuator side are reduced, and the mechanism has larger reachable workspace limits and no interworkspace singularity points. The joints between the links with the carts and the platform are passive universal and passive spherical joints, respectively. This, however, brings the advantage that the platform and the links could be lightweight, which could significantly increase the frequency bandwidth of the mechanism and consequently resulting in high acceleration and velocity.

The position of the spherical joints on the platform and the universal joints on the carts according to the so-called Tau configuration is such that the links within the arms 2 and 3 form vertices of a parallelogram. This creates a constant orientation and a purely translational movement of the platform. Then the three active revolute joints are responsible for the angular configuration of the cockpit by connecting arms 4, 5 and 6. **CCP** is the centre of the cockpit that is connected to the end of the wrist mechanism and **T** is the centre of the moving platform that is connected to the end of the parallel part of the mechanism.

Figure 3(b) shows a CAD model that is developed for this mechanism in the CATIA software environment using the geometric parameters of the Gantry-Tau-3R manipulator with the cockpit, as given in the Appendix. In this design, the length of the passive link is 3 m and the length of the guideways is 3 m. The platform of the mechanism has an angle of 45° with the x-axis of the guideway. The Gantry-Tau manipulator could be easily reconfigured with different link lengths and cart angles.

https://doi.org/10.1017/S0263574719001516 Published online by Cambridge University Press

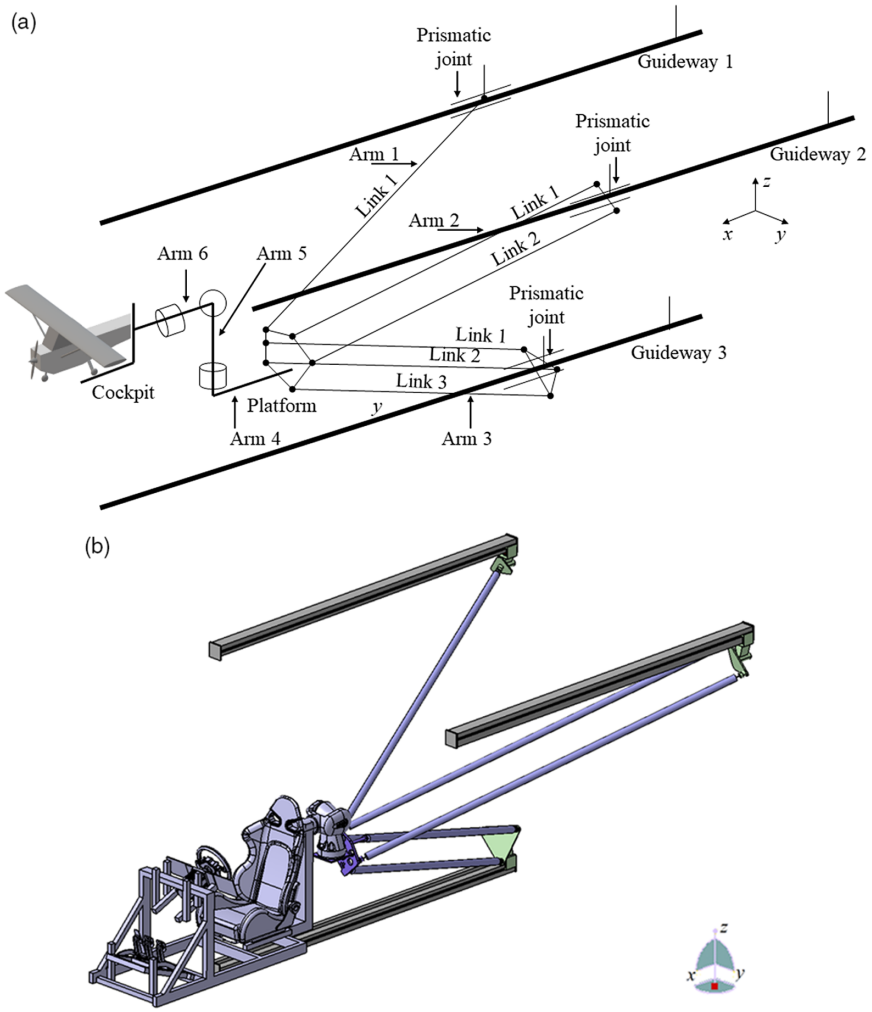

Fig. 3. (a) The schematic model of the Gantry-Tau-3R mechanism and (b) the CAD model.

2.2. Inverse kinematics

The inverse kinematics model of the Gantry-Tau-3R involves the determination of the displacement, velocity and acceleration of the three joints on the guides and three joints on the platform for a given cockpit position, velocity and acceleration.[19] In the literature, the inverse kinematics of the position is provided and the inverse kinematics of the velocity and acceleration are still open research gap in this domain. The forward or direct dynamic is related to the force and inertia of the mechanism, and it is investigated in elsewhere,[18,45] while the active joints' velocities and accelerations are not recalculated.[17,18,46,47] This section is divided into two subsections for the inverse kinematics of the serial part of the mechanism as well as the parallel part of the mechanism.

2.2.1. 3-DoF D1 Gantry-Tau. Figure 4(a) and (b) shows the vector representation of the Gantry-Tau-3R mechanism for both parallel and serial parts of the mechanism. The parallel part of the mechanism called D1 Gantry-Tau[20] is shown in Fig. 4(a). The x-direction of the world coordinate frame $\mathbf{W}$ is assumed to be in the direction of the guideways and its z-axis is vertical. It is also assumed that $\mathbf{A}_i^s$, with $i = 1$–3, is a fixed vector pointing from the origin of the world coordinate frame to the point at the start position of the ith guideway. $\mathbf{q}_i$ is a vector from the starting point of the ith guideway to the position of the prismatic joint on that guideway. $\mathbf{C}_{i,k}$ is also a fixed vector pointing from the position of the prismatic joint on the ith guideway to the kth joint of the ith cart. Here, the subscript k indicates the number of the links in each arm set, and for arm 1 ($i = 1$ and $k = 1$), for arm 2 ($i = 2$ and $k = 1, 2$) and for arm 3 ($i = 3$ and $k = 1, 2, 3$).

https://doi.org/10.1017/S0263574719001516 Published online by Cambridge University Press

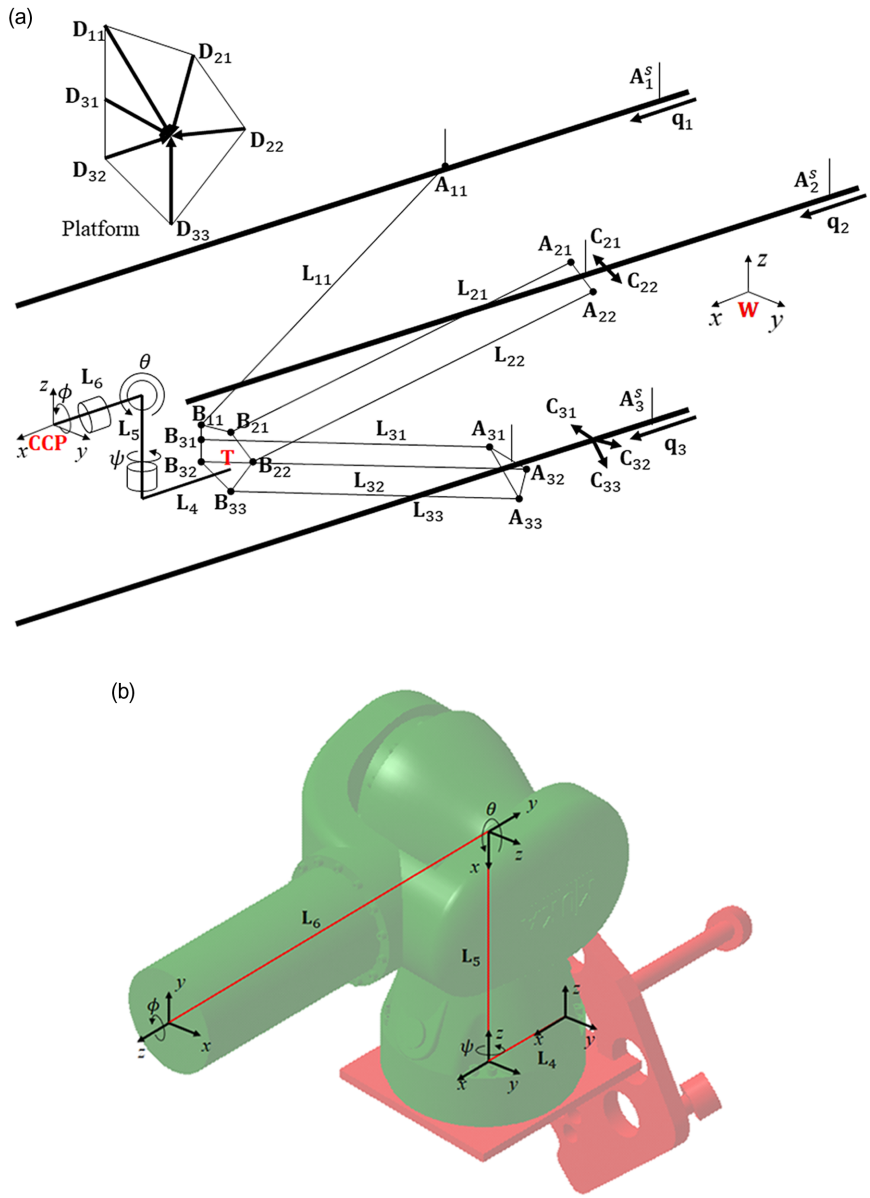

Fig. 4. The vector representation of the Gantry-Tau-3R mechanism (a) parallel part and (b) serial part.

The position of the *k*th universal joint of the *i*th arm is defined in the world coordinate as:

$$\mathbf{A}_{i,k} = \mathbf{A}_i^s + \mathbf{q}_i + \mathbf{C}_{i,k} \tag{1}$$

One characteristic of the D1 Gantry-Tau mechanism is that the positions of the spherical joints on the platform and the universal joints on the carts are such that the links within either arm 2 or 3 form parallelograms. The positions of the universal joints on the cart are fixed, and they only have linear movements because of $\mathbf{q}_i$. This, however, assures that the orientation of the platform will not change with the movement of the active joints. Therefore, the motion of the platform is purely 3D translational. This property simplifies the kinematics model into only translation vectors and does not require rotation transformation. In addition, it is inferred that the vectors between the platform spherical joint positions and any point on the platform will remain with no angular change with the movement of the actuated joints; hence, they are constant vectors. According to Fig. 4(a), $\mathbf{D}_{i,k}$ is a constant vector that relates any of the platform's spherical joints to the origin of platform coordinate frame ($\mathbf{T}$) which is at an arbitrary centre of the platform.

https://doi.org/10.1017/S0263574719001516 Published online by Cambridge University Press

The position of the spherical joints on the platform, $\mathbf{B}_{i,k}$, can be obtained as:

$$\mathbf{B}_{i,k} = \mathbf{A}_i^s + \mathbf{q}_i + \mathbf{C}_{i,k} + \mathbf{L}_{i,k} \tag{2}$$

where $\mathbf{L}_{i,k}$ is the length vector denoting the relationship between the joint on the cart of the kth link of the ith arm, which has a fixed length but variable direction, and can be obtained as:

$$\mathbf{L}_{i,k} = \mathbf{A}_{i,k} - \mathbf{B}_{i,k} \tag{3}$$

T is the position of the **PCF** coordinate frame and can be obtained as follows:

$$\mathbf{T} = \mathbf{B}_{i,k} + \mathbf{D}_{i,k} = \mathbf{F}_i + \mathbf{q}_i + \mathbf{L}_{i,k} \tag{4}$$

where $\mathbf{F}_i = \mathbf{A}_i^s + \mathbf{D}_{i,k} + \mathbf{C}_i^s$, and this vector is constant, as all its components are constant ($\mathbf{F}_i$ is defined because it is constant).

The kinematic constraint for the ith kinematic chain is as follows:

$$\mathbf{L}_{i,k} = \mathbf{T} - \mathbf{F}_i - \mathbf{q}_i \tag{5a}$$

$$\left\|\mathbf{L}_{i,k}\right\|^2 = \left\|\mathbf{T} - \mathbf{F}_i - \mathbf{q}_i\right\|^2 \tag{5b}$$

The below constraints reduce the number from 2 to 1 for the arm 2 and from 3 to 1 for the arm 3 (Eq. (5b)).

$$\mathbf{D}_{2,1} + \mathbf{L}_{2,1} + \mathbf{C}_{2,1} = \mathbf{D}_{2,2} + \mathbf{L}_{2,2} + \mathbf{C}_{2,2} \tag{6a}$$

$$\mathbf{D}_{3,1} + \mathbf{L}_{3,1} + \mathbf{C}_{3,1} = \mathbf{D}_{3,2} + \mathbf{L}_{3,2} + \mathbf{C}_{3,2} = \mathbf{D}_{3,3} + \mathbf{L}_{3,3} + \mathbf{C}_{3,3} \tag{6b}$$

It was mentioned earlier that the vectors $\mathbf{q}_i$ are in the x-direction only, that is, $\mathbf{q}_i = \left[\,(q_i)_x\ 0\ 0\,\right]$. Therefore, the inverse kinematics of position can be obtained as follows:

$$\mathbf{q}_{ix} = T_x - F_{ix} - \sqrt{|\mathbf{L}_i|^2 - \left(F_{iy} - T_y\right)^2 - \left(F_{iz} - T_z\right)^2} \tag{7}$$

where x, y and z indices denote the x, y and z components of the vectors and the negative sign before the square root operators are because q_i is always less than T_x.

$\mathbf{L}_{i,k} = \left[\,L_{i,k_x}\ L_{i,k_y}\ L_{i,k_z}\,\right]$ can also be determined by substituting the joint positions from Eq. (7) into Eq. (5a).

2.2.2. Spherical wrist mechanism. Figure 4(b) demonstrates the spherical wrist mechanism of the Gantry-Tau-3R manipulator, which determines the orientation of the cockpit and is also called the inverse orientation kinematics. The angular positions of the revolute active joints are equal to the angular position of the cockpit. The only problem is to find the linear position of the cockpit known as cockpit centre point (CCP) according to the angular position of the cockpit. The linear position of the cockpit can be obtained as:

$$CCP_x = T_x + (\lceil \mathbf{L}_4 \rceil + |\mathbf{L}_6| \cos\psi \cos\theta\ ) \tag{8a}$$

$$CCP_y = T_y + (|\mathbf{L}_6| \sin\psi \cos\theta\ ) \tag{8b}$$

$$CCP_z = T_z + (|\mathbf{L}_5| - |\mathbf{L}_6| \sin\theta\ ) \tag{8c}$$

where ϕ, θ and ψ are the angular rotation of the cockpit around x-, y- and z-axis known as roll, pitch and yaw. $\mathbf{L}_4$, $\mathbf{L}_5$ and $\mathbf{L}_6$ are the vectors of the arms 4, 5 and 6. The calculated position of the cockpit should be updated to the inverse kinematic part of the parallel to find the proper position of the prismatic joints.

3. Control of Gantry-Tau-3R-Based SBMPs

3.1. PID controller

The PID controller is widely used in industrial applications as a control loop feedback mechanism because of its easy tuning, cost-effective and practical features.[48] An error value known as *e(t)* calculated by the PID controller shows the difference in the desired value and a measured value using the sensors and applies the control correction action by proportional, integral and derivative terms know

https://doi.org/10.1017/S0263574719001516 Published online by Cambridge University Press

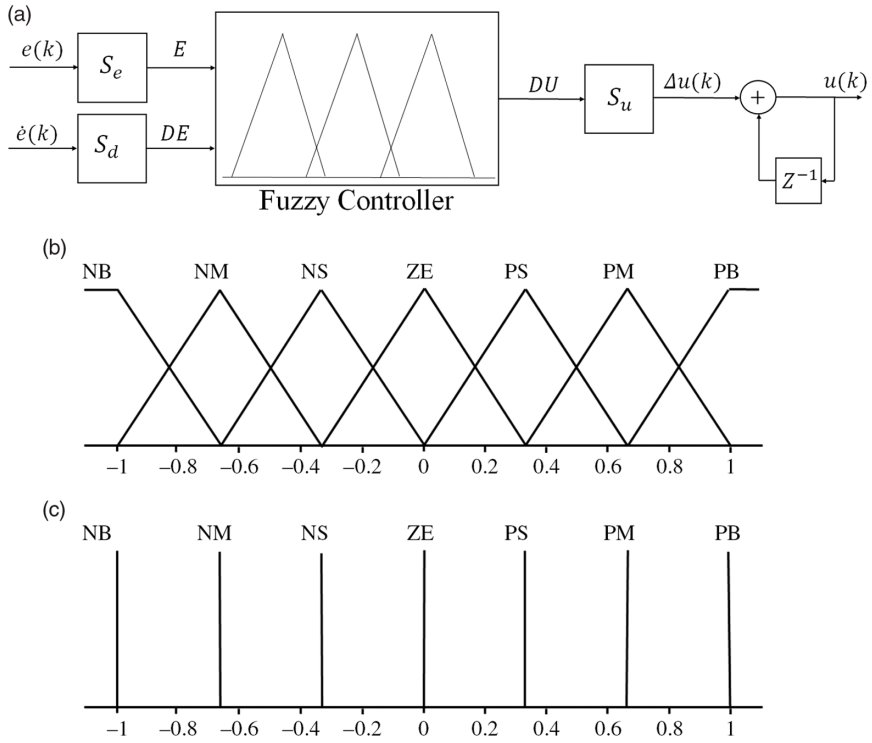

Fig. 5. (a) The structure of two input FIC for a Gantry-Tau-3R, (b) input membership functions of weight factor for active joints error and variation of error, and (c) output membership functions of control action.

as P, I and D, respectively. These are the gains of the PID controller which should be tuned properly to reach the lowest tracking error. GA is employed in this study to calculate the optimum PID gains. GA is a heuristic and robust search technique that can solve nonlinear and complex problems with less chance of falling into local minima, while searching for the best possible solution.[49,50]

3.2. FIC controller

The fuzzy logic theory was introduced by Zadeh,[51] and it has found its place in control concepts from the beginning.[29–32] The fuzzy logic system is one of the best techniques for nonlinear systems with stochastic behaviour and inconstant inputs. Figure 5(a) shows the structure of the two-input FIC for the hexarot manipulator. In Fig. 5(a), $e\,(k)$ and $\dot{e}\,(k)$ are the errors of active joint position and change in error in the kth sampling time, respectively.

The $\dot{e}\,(k)$ can be calculated as:

$$\dot{e}\,(k) = \frac{e\,(k) - e\,(k-1)}{T_s} \tag{9}$$

where T_s and $e\,(k-1)$ are the sampling time and the error of active joint positions in the $(k-1)$th sampling time.

The input and output of the FIC should be normalised inside the $[-1, 1]$ interval. The linear gains known as S_e, S_d and S_u are employed to normalise the input and output of the FIC inside the discourse of $[-1, 1]$. These linear gains are tuned by GA to reduce the joint space tracking error as much as possible.

Table I shows the GA adjustments . The parameters of GA should be chosen properly to increase the accuracy and convergence speed of the solution. The suitable settings of the crossover and mutation rates guarantee the success of GA and extracted results.[52–57] The high mutation rate increases the risk of missing the solution close to the current situation. Also, the low mutation rate can lead to be stuck in the local optimum position. The population size of the study is chosen to be 80. The low population size limits the search capability of GA. On the other hand, the high population size increases the optimisation time without any noticeable improvement in the results.[58] The obtained

https://doi.org/10.1017/S0263574719001516 Published online by Cambridge University Press

Table I. GA adjustment parameters for FIC.

Parameters	**Value**
Variables	18
Population size	100
Maximum generation	50
Crossover rate	0.8
Mutation function	Adaptive feasible
Function tolerance	10^{-4}

Table II. Linear gains of the controllers.

Controller	K_P **or** S_e	K_I **or** S_u	K_D **or** S_d
PID	$[7.5; 6.25; 12.5; 15; 8.75; 2] \times 104$	$[9; 8; 15; 19; 11; 3] \times 102$	$[2; 2; 2; 1; 3.5; 1.2] \times 103$
FIC	$[1; 1; 1; 1; 1; 1]$	$[58; 73; 61; 84; 65; 71]$	$[7.2; 8; 9; 8; 8.7; 9.7]$

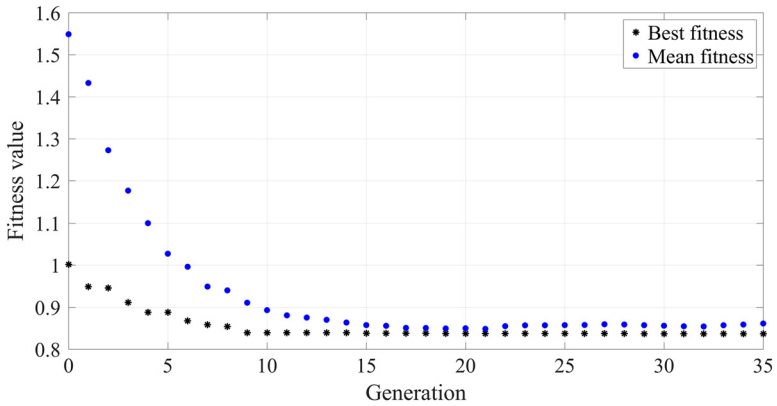

Fig. 6. The genetic convergence of the FIC.

results of GA prove that the parameters including mutation rate, crossover friction, population and generation have been properly selected for the problem. Figure 6 shows the genetic convergence to find the best solution for minimising the motion tracking error. In regard to the fuzzy controller rules and membership functions, it should be noted that the membership functions of the FIC are chosen based on the maximum experienced values during the flying tests and number of rules selected by our knowledge acquired from the problem and mechanism aiming to achieve in a desirable output.[30]

The extracted values are reported in Table II. According to the linear gains of the FIC, the normalised inputs and output of the FIC can be calculated as follows:

$$\triangle u\,(k) = S_u DU \tag{10a}$$

$$\mathrm{E} = S_e e\,(k) \tag{10b}$$

$$\mathrm{DE} = S_d \dot{e}\,(k) \tag{10c}$$

where $\triangle u\,(k)$ is the change in the control action in the kth sampling time. Also, DU, E and DE are the normalised value of the control action change, the error of active joints positions and the change in the error in the active joints position, respectively.

In order to find the control action in the kth sampling time, the new output should be added to the past output. Then the control action in the kth sampling time is as follows:

$$u\,(k) = u\,(k-1) + \triangle u\,(k) \tag{11}$$

where $u\,(k-1)$ is the control action of the FIC in the $(k-1)$th sampling time.

The Sugeno-type fuzzy blocks and triangular and singleton membership functions are chosen to decrease the tracking error of the moving platform as input and output, respectively. The input

https://doi.org/10.1017/S0263574719001516 Published online by Cambridge University Press

Table III. Fuzzy logic rules for the calculation of the control action.

DU	**E**						
DE	NB	NM	NS	ZE	PS	PM	PB
NB	NB	NB	NB	NB	NM	NS	ZE
NM	NB	NB	NB	NM	NS	ZE	PS
NS	NB	NB	NM	NS	ZE	PS	PM
ZE	NB	NM	NS	ZE	PS	PM	PB
PS	NM	NS	ZE	PS	PM	PB	PB
PM	NS	ZE	PS	PM	PB	PB	PB
PB	ZE	PS	PM	PB	PB	PB	PB

weight parameters for the normalised error and error variation are divided within seven membership functions such as negative big (NB), negative medium (NM), negative small (NS), zero (ZE), positive small (PS), positive medium (PM) and positive big (PB) (Fig. 5(b)). Also, the membership function of the control action is categorised into seven singleton membership function, namely, NB, NM, NS, ZE, PS, PM and PB (Fig. 5(c)). The fuzzy logic rules should be determined after the calculation of the normalised input and output. The rules are defined systematically because the platform starts moving from a neutral position to minimise the error of the platform with the definition of the 49 rules shown in Table III.

4. Linear MPC-Based MCA Using Human Vestibular System Model

In this section, the MPC-based MCA is explained. Initially, the human vestibular system is studied to extract the MPC-based MCA according to the human vestibular model.

4.1. Human vestibular model

The human motion perceptual system is the set of biological systems and organs that can sense information about the environment. The motion perception consists of three systems including the visual system, the auditory system, tactile organ and the vestibular system. We focus on the vestibular model rather than the first two systems because the SBMP motions reproduce this system. The vestibular system is positioned inside the inner ear and includes the semicircular canals and otolith organs. The vestibular system senses the angular and linear motions.[59–61] The otolith organs perceive the specific force by translational acceleration minus gravity acceleration, as below:

$$\mathbf{S}_F = \mathbf{a} - \mathbf{g} \tag{12}$$

if $\mathbf{R}$ is a rotation matrix of the SBMP's end effector, the sensed specific force in the centre of the SBMP's end effector can be formulated as:[62]

$$\mathbf{S}_F = \mathbf{a} - \mathbf{R}\,(\phi, \theta, \psi)\,\mathbf{g} = \begin{bmatrix} a_x + g\,\sin\theta \\ a_y - g\,\sin\phi\,\cos\theta \\ a_z - g\,\cos\phi\,\cos\theta \end{bmatrix} \tag{13}$$

The different mathematical model of the otolith organs are analysed in elsewhere.[59,60] In this research, the most appropriate transfer function model of the otolith organs is elected to reach the better result. Then the best relation of the sensed particular force in the SBMP with the stimulus-specific force can be determined as[59] below:

$$\frac{\hat{f}\,(s)}{f\,(s)} = K_{OTO}\left(\frac{(\tau_a s + 1)}{(\tau_L s + 1)\,(\tau_s s + 1)}\right) \tag{14}$$

where $\tau_L = 5.3\ (s)$ in the x-direction, $\tau_L = 5.33\ (s)$ in y- and z-direction is a long-time constant of the otolith organs. $\tau_s = 0.016\ (s)$ and $\tau_a = 13.2\ (s)$ in three directions are short-time constant of the otolith organs and neural processing term lead operator. Also, $K_{OTO} = 0.4$ shows the human threshold unit.

The transfer function model of the human semicircular system is compared elsewhere,[60,61] and the best mathematical model of them has been chosen in this study to reach the reasonable results as below:

https://doi.org/10.1017/S0263574719001516 Published online by Cambridge University Press

$$\frac{\widehat{\omega}\,(s)}{\omega\,(s)} = K_{OTO}\left(\frac{\tau_1\tau_a s^2}{(\tau_a s+1)\,(\tau_1 s+1)}\right) \tag{15}$$

where $\tau_1 = 5.3\ (s)$ in the x-direction, $\tau_1 = 6.1\ (s)$ in the y-direction, $\tau_1 = 10.2\ (s)$ in the z-direction is a long-time constant and $\tau_a = 30\ (s)$ in three directions are adaption time constants.

4.2. The MPC-based MCA

The continued state space model should be discretised in a sampling time to be employed in MPC model as follows:

$$\mathbf{x_m}\,(t+1) = \mathbf{A_m x_m}\,(t) + \mathbf{B_m}\,\mathbf{u_m}(t) \tag{16a}$$

$$\mathbf{y}\,(t) = \mathbf{C_m x_m}\,(t) \tag{16b}$$

The variation in the inputs should be found as it involves boundaries on the inputs' rates, inputs and outputs.

$$\triangle\mathbf{u}\,(t) \triangleq \mathbf{u}\,(t) - \mathbf{u}\,(t-1) \tag{17}$$

At the same way, the variation in the state is calculated as follows:

$$\triangle\mathbf{x_m}\,(t) \triangleq \mathbf{x_m}\,(t) - \mathbf{x_m}\,(t-1) \tag{18}$$

According to the newly defined variables via Eqs. (17) and (18), the new augment state space model is defined as:

$$\mathbf{x}\,(t+1) = \begin{bmatrix} \mathbf{A_m} & \mathbf{0} \\ \mathbf{C_m A_m} & \mathbf{I} \end{bmatrix}\mathbf{x}\,(t) + \begin{bmatrix} \mathbf{B_m} \\ \mathbf{C_m B_m} \end{bmatrix}\triangle\mathbf{u}(t) \tag{19a}$$

$$\mathbf{y}\,(t) = \begin{bmatrix} \mathbf{0}\ \mathbf{I} \end{bmatrix}\mathbf{x}\,(t) \tag{19b}$$

where $\triangle\mathbf{u}$ is the control input. $\mathbf{A}$, $\mathbf{B}$ and $\mathbf{C}$ are defined as the new augment's matrices:

$$\mathbf{A} = \begin{bmatrix} \mathbf{A_m} & \mathbf{0} \\ \mathbf{C_m A_m} & \mathbf{I} \end{bmatrix},\ \mathbf{B} = \begin{bmatrix} \mathbf{B_m} \\ \mathbf{C_m B_m} \end{bmatrix},\ \mathbf{C} = \begin{bmatrix} \mathbf{0}\ \mathbf{I} \end{bmatrix} \tag{20}$$

With definition of $\mathbf{R_s}$ which is the reference signal including sensed angular velocity and sensed specific force by real driver, the cost function is calculated as:

$$\mathbf{J}\,(\triangle\mathbf{U}) = (\mathbf{R_s} - \mathbf{Y})^T\mathbf{Q}\,(\mathbf{R_s} - \ \mathbf{Y}) + \mathbf{U}^T\mathbf{S}\mathbf{U} + \triangle\mathbf{U}^T\mathbf{R}\triangle\mathbf{U} \tag{21}$$

where $\mathbf{Q}$, $\mathbf{S}$ and $\mathbf{R}$ are the weighting matrices of the cost function to castigate the outputs, inputs and inputs' rates. The restrictions of outputs, inputs and inputs' rates are categorised in three groups as $\mathbf{M}_1$, $\mathbf{n}_1$; $\mathbf{M}_2$, ; and $\mathbf{M}_3$ and $\mathbf{n}_3$, and they are defined to consider in a QP problem as below:

$$\begin{bmatrix} \mathbf{M}_1 \\ \mathbf{M}_2 \\ \mathbf{M}_3 \end{bmatrix}\triangle\mathbf{U} \leq \begin{bmatrix} \mathbf{n}_1 \\ \mathbf{n}_2 \\ \mathbf{n}_3 \end{bmatrix} \tag{22}$$

The MPC-based MCA is decoupled in four separate modes including longitudinal, lateral, yaw and heave modes to make the fast implementation of the MPC. The workspace limitations of the proposed Gantru-Tau-3R mechanism is shown in Table IV. It is obvious that the proposed manipulator is capable of following the signals with larger linear and angular displacement compared to the parallel and serial manipulators. The MPC-based MCA are tuned using the trial-and-error method to have the best usage of the workspace. Initially, the prediction and control horizons are chosen according to the computational burden of the hardware and then the weights are balanced to restrict the maximum tracking error for sensed specific force and sensed angular velocity between the pilots in the real airplane and the SBMP. Finally, the input signals are scaled down to not exceeding the workspace limitations (Table V).

Unfortunately, the common parallel and serial manipulators are not appropriate choices for the MPC-based MCA due to the restricted angular or linear displacement of the moving platform, respectively. On the other hand, the proposed Gantry-Tau-3R is capable of larger linear and angular

https://doi.org/10.1017/S0263574719001516 Published online by Cambridge University Press

Table IV. The workspace limitations of the Gantry-Tau-3R manipulator.

Index	**Gantry-Tau-3R**
X (meter)	±1
Y (meter)	±1
Z (meter)	±1
Roll (degree)	±360
Pitch (degree)	±60
Yaw (degree)	±90

Table V. The tuning parameters of the MPC-based MCA for the proposed Gantry-Tau-3R manipulator.

Parameters	**Longitudinal**	**Lateral**	**Yaw**	**Heave**
Translational scale factor	1/2	1/2	–	1/2
Angular scale factor	1	1	1	–
Control horizon	150	150	150	100
Prediction horizon	3	3	3	3
Wight of sensed specific force	350	400	–	125
Weight of translational displacement	290	650	–	200
Weight of translational velocity	5	5	–	25
Weight of translational acceleration	0.0001	0.0001	–	0.0001
Weight of translational jerk	1	1	–	0.0001
Weight of sensed angular velocity	2000	1400	1700	–
Weight of angular displacement	0.001	0.001	300	–
Weight of angular velocity	0.1	0.1	0.0001	–
Weight of angular acceleration	1	1	0.0001	–

displacement as a high-G SBMP due to the unique structure of the proposed mechanism. The parallel part of the newly proposed mechanism is capable of handling the linear movement of the cockpit, and the serial part of the mechanism known as spherical wrist mechanism is capable of handling the large angular displacement of the cockpit. Therefore, the proposed mechanism takes the advantages of both parallel and serial mechanisms while eliminating their weak points. As it is obvious, the parallel manipulator suffers from the restricted angular displacement, and serial manipulator suffers from the limited linear displacement of the end effector inside the workspace because of the isomeric configuration of the joints.

5. SimMechanic Modelling

In this section, the Simulink model of the Gantry-Tau-3R SBMP with respect to the PID and FIC as well as MPC-based MCA is modelled and implemented in MATLAB software. It consists of the MPC-based MCA, the inverse kinematics,[63] controller[48] and SimMechanic units.

The MPC-based MCA is used to find the motion signals to reproduce the motion sensation as realistic as possible to the real vehicle according to the provided model in Section 4. It is able to consider the physical and dynamical limitation of the mechanism. By the way, the computational burden of the MPC is a big concern in a practical case in real-time mechanisms. The implemented MPC-based MCA is very fast and can be used real time as qpOASES algorithm[64] can be used to solve the quadratic program of the MPC with consideration of the 0.1 s for the time step.

Then the inverse kinematic block is responsible for the calculation of the desired positions of the active joints according to the configuration of the cockpit.[19,65] This block is modelled according to the kinematic model of the mechanism discussed in Section 2.

The controller unit perceives the extracted active joint positions. The proposed PID and FIC mentioned in Section 3 are modelled in this block. Their gains are designed and tuned using GA to reach the minimum tracking error of the active joints while keeping the stability of the controller (Table II). The fitness function of the GA is defined below for 2 s of the motion with a sinusoid signal in six channels:

$$E = \frac{1}{6}\sum_{i=1}^{6}(|e_i(k)|) \tag{23}$$

https://doi.org/10.1017/S0263574719001516 Published online by Cambridge University Press

where e_i is the error of the ith active joints in the kth sampling time. Also, the mutation function and crossover rate are adaptive feasible and 0.8, respectively, with 100 population (Table I).

The human vestibular model is modelled in the Simulink which is used to find the motion sensation error between the real pilot and the user of SBMP. The SimMechanic model which is shown in Fig. 7 is used to find the response of the SBMPs to the different motion scenarios while working along with the MPC-based MCA using PID and FIC.

6. Results and Discussions

The Simulink's input signals are captured through the flight simulation environment called Xplan11 for 175 s as shown in Fig. 8(a)–(c) for take-off and flying scenario. Figure 8(a) shows the flying route of the Cessna 172 Skyhawk during the 175 s of the flight scenario including the take-off scenario with two roll manoeuvres. The linear acceleration and angular velocity signal after implementation of the translational and angular scale factors are shown in Fig. 8(b) and (c) for 175 s of the flight scenario. The scale factor (Table V) is defined to keep the moving platforms within the limitations of the SBMP and allow the MPC-based MCA to produce more accurate motion signals for generating accurate flying motion sensation for the SBMP's user. With consideration of the Simulink/MATLAB model as a real SBMP with traditional PID and FIC, the proposed model in MATLAB can compare the results for proposed Gantry-Tau-3R with traditional PID and FIC. In addition, the ability of the newly designed Gantry-Tau-3R mechanism in regeneration of the larger motion signals with higher linear acceleration and angular velocity is compared with Stewart platform as a common SBMP.

Figure 9(a)–(f) shows the sensed angular velocity and sensed specific force along x-, y- and z-axis for the pilot of the real airplane as well as the users of Stewart platform and Gantry-Tau-3R. Figure 9(a)–(c) shows the sensed angular velocity along roll-, pitch- and yaw-angles using Stewart platform and Gantry-Tau-3R. The results show the reliability of the sensed angular velocity via the newly designed Gantry-Tau-3R due to its capability in regenerating larger angular displacement compared with common Stewart platform. In addition, the sensed specific force of the SBMP's driver improves with Gantry-Tau-3R based on to the better reproduction of the high-frequency and low-frequency signals due to the combination of parallel and serial structures.

The sensed angular velocity and sensed specific force along x-, y- and z-axis are shown in Fig. 10(a)–(f) for the actual airplane in the real world and the SBMP with PID and FIC. Figure 10(a)–(c) shows the sensed angular velocity for longitudinal, lateral, heave channels with real airplane and proposed SBMP with PID and FIC. According to Fig. 10(a)–(c), the sensed angular velocity of the proposed SBMP with FIC is highly reliable with less false motion cues compared to traditional PID controller. It makes the more realistic flying feel by reducing the tracking error of the moving platform with high-frequency angular velocity signals. Figure 10(d)–(f) shows the reduction in the sensed specific force by the proposed SBMP using the FIC because of the capability of following the high-frequency angular velocity signals. Also, the proposed SBMP is able to follow large signals such as 5 m/s^2 as shown in Fig. 10(e) because of largely available workspace compared to normal parallel and serial SBMPs. Also, the reason for the fluctuation at the beginning of the motion is due to the motion of the end effector from the neutral position that normally takes 0.1 s to compensate the cockpit gravity.

Figure 11(a)–(c) shows the error of the sensed angular velocity along the x-, y- and z-axis between the real and the Gantry-Tau-3R SBMP using traditional PID and the proposed FIC. The proposed SBMP with FIC reduces the error of the sensed angular velocity due to the high capability of producing angular displacement. For instance, the error of sensed angular velocity for the longitudinal channel reduces from 0.2311 rad/s to 0.2022 via FIC compared to the traditional PID controller. Also, Fig. 11(d)–(f) shows the error of the sensed specific force along the x-, y- and z-directions between the real vehicle and SBMP users using the two controllers. The reduction in the sensed specific force error using the proposed Gantry-Tau-3R SBMP with FIC proves the efficiency of the proposed SBMP with FIC. The maximum sensed specific force error in the longitudinal direction is less than 3.385 m/s^2 using the proposed SBMP, while it is 3.601 m/s^2 for the traditional PID controller.

In the next step, the results of the captured flight scenario using traditional PID and FIC are listed in Table VI. Root mean square error (RMSE) indicates the sensed specific force and sensed angular velocity between the pilot in the real airplane and the pilot in the SBMPs. It is shown that the human

https://doi.org/10.1017/S0263574719001516 Published online by Cambridge University Press

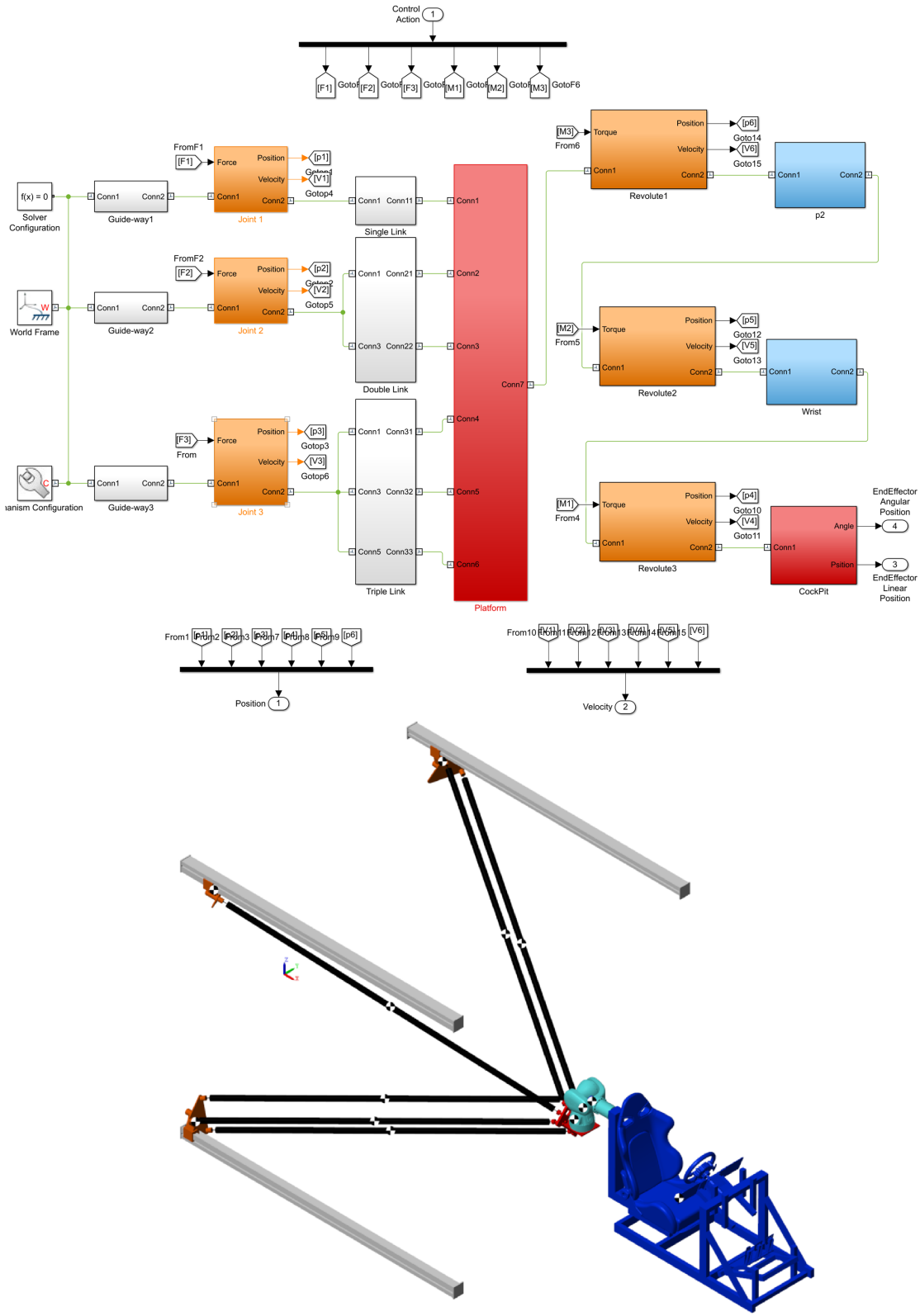

Fig. 7. The SimMechanic model of the Gantry-Tau-3R using the Simulink of MATLAB software.

sensation error decreases using the Gantry-Tau-3R with FIC, as the FIC is capable of providing high tracking performance of the moving platform due to the structure of the fuzzy mechanism. The second part of Table VI presents the correlation coefficient (CC) factor[66–68] to show and compare

https://doi.org/10.1017/S0263574719001516 Published online by Cambridge University Press

Table VI. The result of the proposed Gantry-Tau-3R high-G SBMP with PID and FIC.

	RMSE		CC	
Index	**PID**	**FIC**	**PID**	**FIC**
Error of longitudinal sensed specific force	0.2680 (m/s^2)	0.2184 (m/s^2)	0.9166	0.9330
Error of lateral sensed specific force	0.5233 (m/s^2)	0.4474 (m/s^2)	0.9527	0.9632
Error of vertical sensed specific force	0.4621 (m/s^2)	0.4582 (m/s^2)	0.0345	0.0456
Error of sensed angular velocity (x-axis)	0.0373 (rad/s)	0.0320 (rad/s)	0.8591	0.8663
Error of sensed angular velocity (y-axis)	0.0347 (rad/s)	0.0287 (rad/s)	0.5523	0.6375
Error of sensed angular velocity (z-axis)	0.0179 (rad/s)	0.0166 (rad/s)	0.9414	0.9494

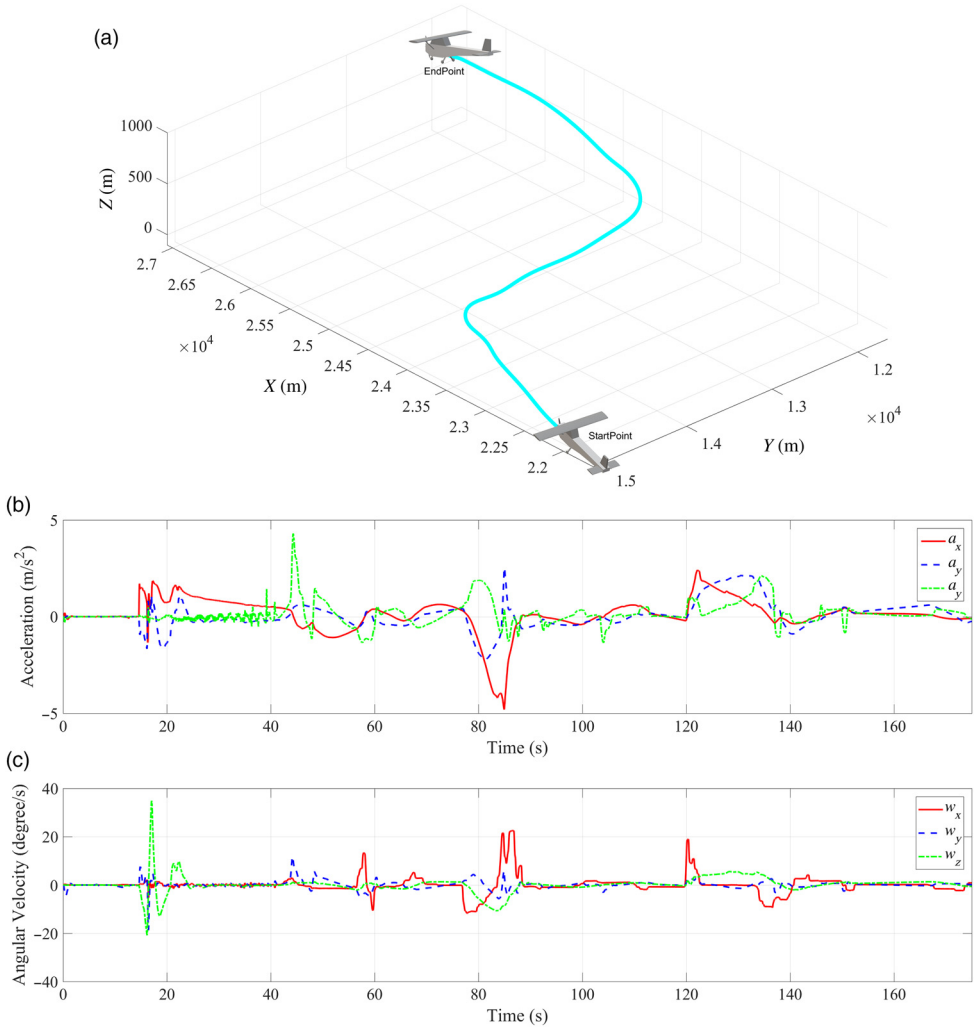

Fig. 8. The reference signal (real airplane motions): (a) airplane path, (b) linear acceleration and (c) angular velocity.

the shape similarity in motion sensation between the SBMP user SBMP and the real pilot of the airplane.[1,30] According to the results, it is clear that the Gantry-Tau-3R high-G SBMP using FIC can follow the shape of the reference signal more precisely compared with the same SBMP using traditional PID controller. The error of sensed specific force RMSE in x-, y- and z-direction of the proposed Gantry-Tau-3R high-G SBMP using FIC is 18, 14 and 0.8% lower than Gantry-Tau-3R high-G SBMP using traditional PID controller. The improvement along x- and y-axis are remarkable,

https://doi.org/10.1017/S0263574719001516 Published online by Cambridge University Press

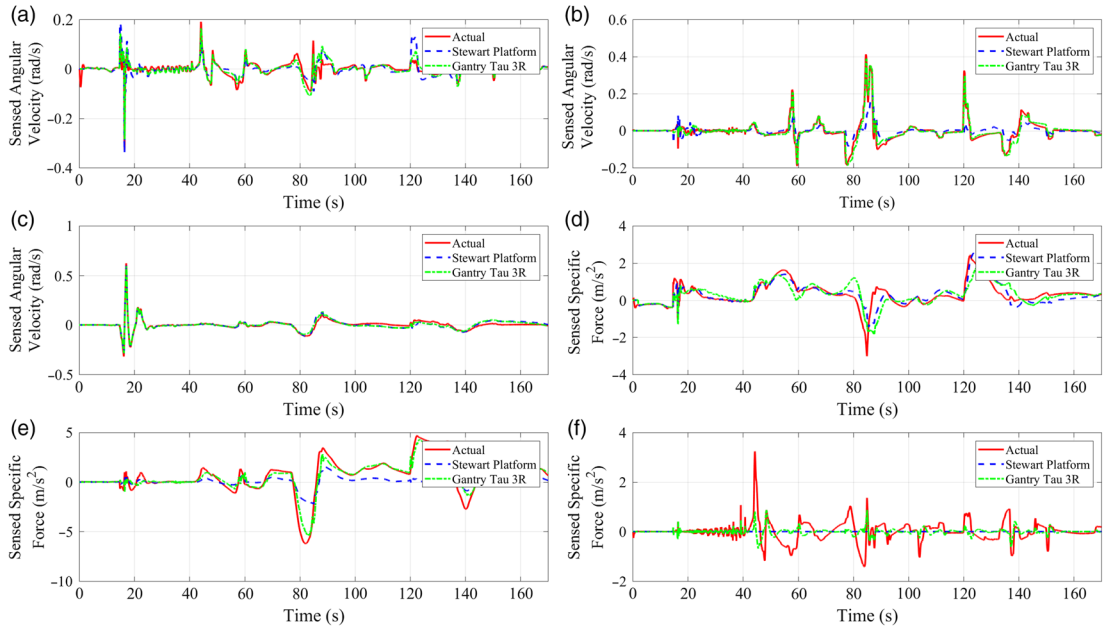

Fig. 9. The sensed angular velocity and specific force for the actual vehicle, common Stewart platform and proposed Gantry-Tau-3R manipulator along: (a) roll-angle, (b) pitch-angle, (c) yaw-angle, (d) *x*-axis, (e) *y*-axis and (f) *z*-axis.

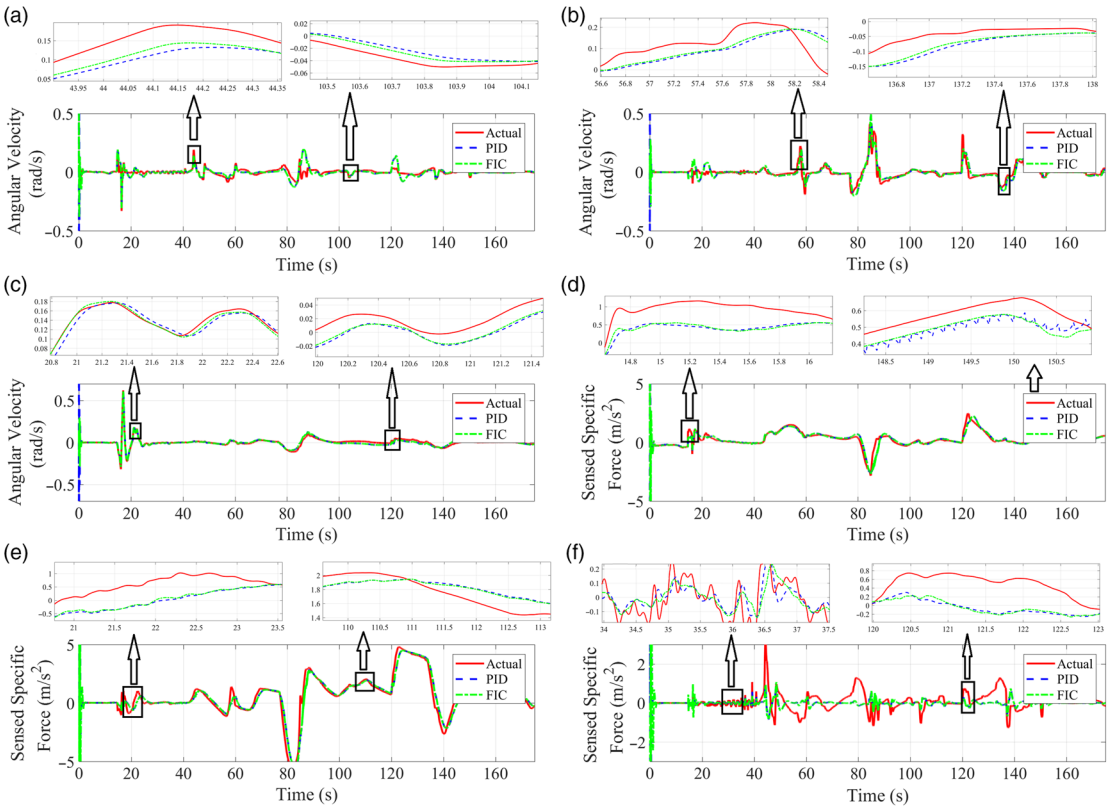

Fig. 10. The sensed angular velocity and specific force for the actual vehicle and newly designed Gantry-Tau-3R manipulator using PID and FIC along (a) roll-angle, (b) pitch-angle, (c) yaw- angle, (d) *x*-axis (e) *y*-axis and (f) *z*-axis.

https://doi.org/10.1017/S0263574719001516 Published online by Cambridge University Press

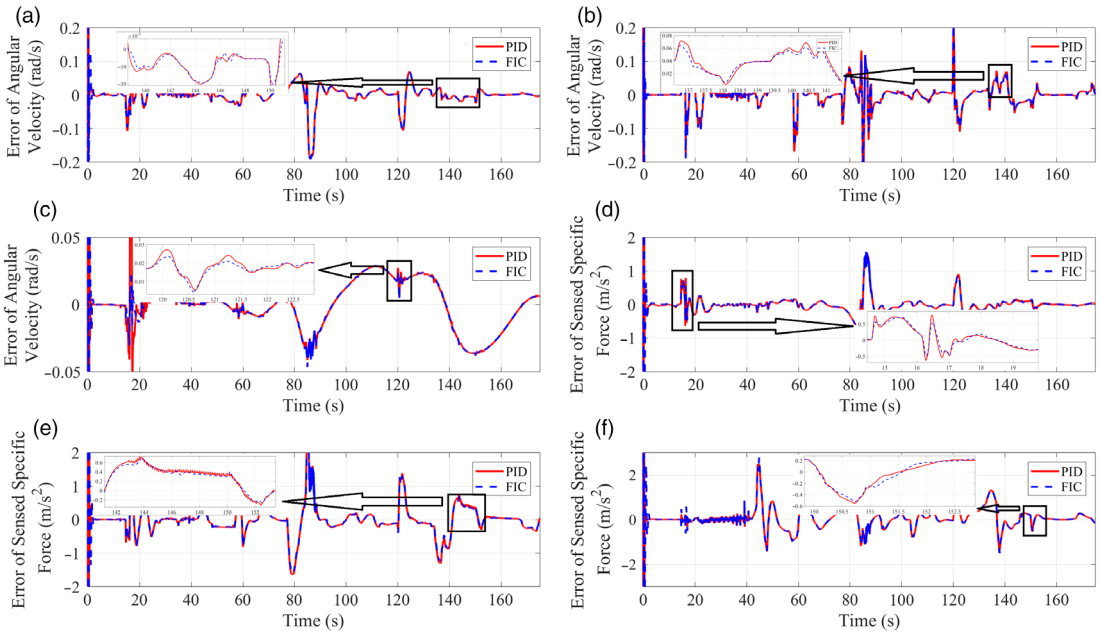

Fig. 11. The error of sensed angular velocity and specific force for the actual vehicle and newly designed Gantry-Tau-3R manipulator using PID and FIC along: (a) roll-angle, (b) pitch-angle, (c) yaw-angle, (d) x-axis, (e) y-axis and (f) z-axis.

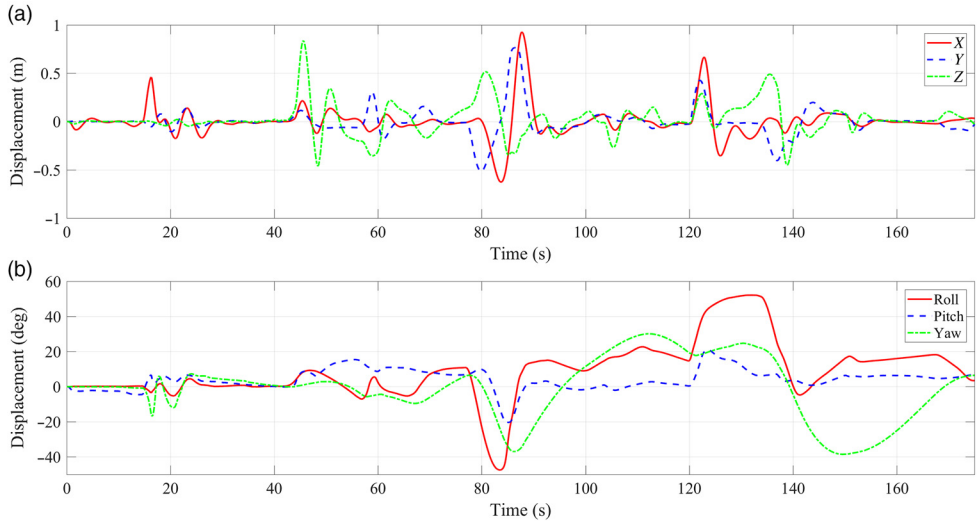

Fig. 12. The displacement of the cockpit during the flight scenario for Gantry-Tau-3R using FIC: (a) linear displacement and (b) angular displacement.

while the improvement along z-axis is negligible. The CC between two signals $y_1\ (t)$ and $y_2\ (t)$ can be found as:

$$\mathrm{CC} = \frac{\mathrm{Cov}\ (y_1\ (t)\ ,\ y_2\ (t))}{\sigma_{y_1} \cdot \sigma_{y_1}} \tag{24}$$

where σ_{y_i} is the standard deviation of y_i. The shape following factor (CC) of the sensed specific force in x- and y-axis changed from 0.9166 to 0.9330 and 0.9527 to 0.9632 with noticeable improvement in the proposed Gantry-Tau-3R high-G SBMP using FIC compared with Gantry-Tau-3R high-G SBMP using the traditional PID controller. In addition, the improvement in sensed specific force along z-axis using Gantry-Tau-3R high-G SBMP with FIC is not remarkable from 0.0345 to 0.0456 as mentioned in RMSE.

https://doi.org/10.1017/S0263574719001516 Published online by Cambridge University Press

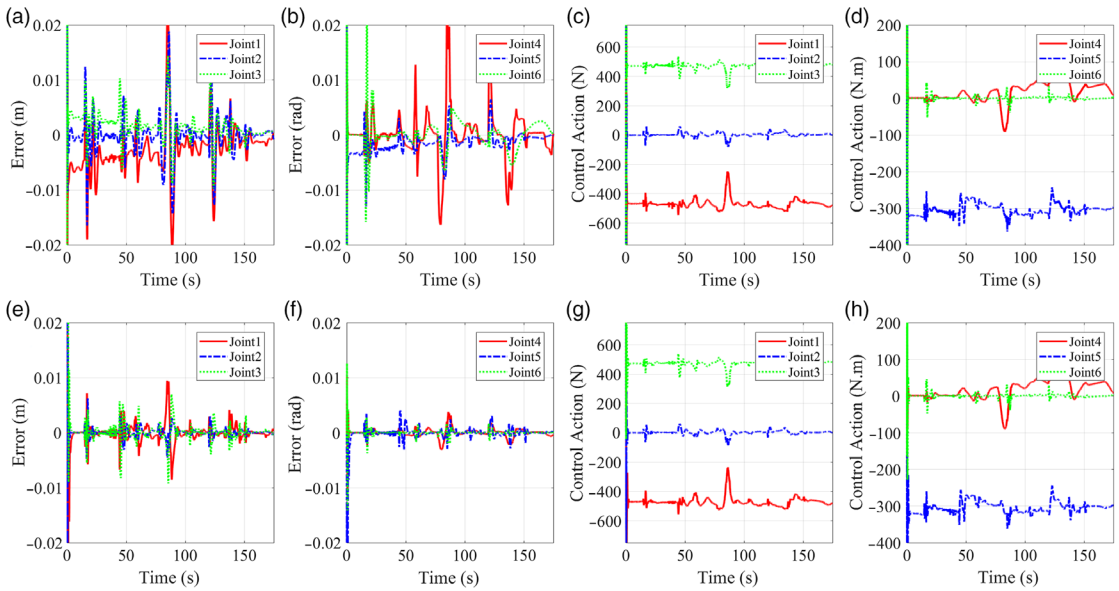

Fig. 13. The joint space errors and control actions of Gantry-Tau-3R: (a) joint space error of prismatic joints with PID controller, (b) joint space error of revolute joints with PID controller, (c) control action of prismatic joints using PID controller, (d) control action of revolute joints using PID controller(e) joint space error of prismatic joints using FIC, (f) joint space error of revolute joints using FIC, (g) control action of prismatic joints with FIC and (h) control action of revolute joints with FIC.

Figure 12(a) and (b) show the SBMP angular and linear displacement around x-, y- and z-direction, respectively, for the proposed Gantry-Tau-3R high-G SBMP using FIC. The proposed SBMP is capable of high linear and angular displacement due to the unique structure of the mechanism with a combination of parallel and serial mechanisms to do the largest linear and angular surge. The proposed mechanism is capable of ± 1 m linear displacement around three directions and large angular displacement, that is, even $\pm 2\pi$ radian for the roll that is necessary for flight scenarios.

Figure 13(a)–(h) shows the active joint space error and control actions of the proposed Gantry-Tau-3R SBMP with both traditional PID and the proposed FIC. Figures 12(e) and 13(a) show the joint space error of the active prismatic joints for the Gantry-Tau-3R manipulator with both PID and the proposed FIC. The FIC reduces the joint space error of the Gantry-Tau-3R manipulator more than 2.5 times for the prismatic joints. Also, Figs. 12(b) and 13(f) show the reduction in the joint space error for the active revolute joints more than eight times. The reduction in the tracking error of the moving platform improves the motion fidelity of the proposed SBMP using FIC.

According to the provided results, the proposed Gantry-Tau-3R using FIC is a very suitable device as a high-G SBMP. It is able to produce high-frequency motions and is highly capable of producing large linear acceleration and angular velocity signals due to the unique structure of the proposed SBMP. Normally, the large signals should be scaled properly not to exceed the workspace limitation with common parallel or serial SBMPs, but the proposed Gantry-Tau-3R does not need the large-scale factor because of its large workspace limitations. In addition, the proposed Gantry-Tau-3R using FIC is an effective tool for generating the realistic motion sensation for the SBMP's users.

7. Conclusions

In this study, Gantry-Tau-3R high-G SBMP using PID and FIC is proposed to work along with an MPC-based MCA for producing the flying motion sensation for the users. The traditional 3-DoF Gantry-Tau manipulator is not able to follow the motion signals due to the limited angular displacement. In this study, for the first time, the inverse kinematic model of the newly designed Gantry-Tau-3R is developed. The common parallel and serial manipulators have large workspace limitations as well as restricted angular displacement of the moving platform, leading to low fidelity motions using the MPC-based MCA. Then the regeneration of the large motion more than 5 m/s^2 as a linear acceleration is not possible using common parallel and serial manipulator such as Stewart platform.

https://doi.org/10.1017/S0263574719001516 Published online by Cambridge University Press

The proposed Gantry-Tau-3R manipulator is a combination of parallel and serial mechanisms to take into account the advantages of both mechanisms. It has a larger linear workspace limitation besides the high available angular displacements of the moving platform due to the additional serial spherical wrist mechanism. With the advantage of inverse kinematics model, the PID and FIC are designed for the mechanism using GA. The PID controller is the most common controller and has many industrial applications because it is cost-effective and easy for tuning, but it is not able to follow the high-frequency signals such as unknown flight scenarios. The low tracking error is important in the concepts of the SBMPs to improve the motion fidelity and prevent the motion sickness caused by the wrong motion cues. As a result, the FIC was modelled and implemented initially to reduce the tracking error of the moving platform and the error of the active joint positions inside the control unit of the manipulator. The MPC-based MCA is modelled and implemented for the proposed Gantry-Tau-3R manipulator by considering the human vestibular model. The proposed Gantry-Tau-3R manipulator is modelled using MATLAB/Simulink software. The results of this study proved the improvement in the proposed Gantry-Tau-3R using FIC in terms of path tracking compared to PID controller by implementing the flight scenario signals in 6 DoF. Also, the proposed mechanism is capable of following large motion signals because of its unique structure. The increase in sensation shape following factor for the generated motion in SBMP and the decrease in sensed motion error between the real pilot and SBMP's pilot prove the effectiveness of the proposed Gantry-Tau-3R SBMP using FIC compared to the traditional PID controller for the flight simulation.

The dynamic analysis and practical evaluation of the proposed mechanism using FIC can be investigated as a future to show the effectiveness of the proposed mechanism. The machine learning and artificial intelligent-based techniques have been recently used for different applications including text mining,[69–72] medicine,[73–76] business[77–80] and robotics.[81] For the future work, the applications of neural network-based controller can be investigated.

References

1. H. Asadi, S. Mohamed, C. P. Lim and S. Nahavandi, "Robust optimal motion cueing algorithm based on the linear quadratic regulator method and a genetic algorithm," *IEEE Trans. Syst. Man Cybern. Syst.* **47**(2), 238–254 (2017).
2. D. Haward, "The sanders teacher," *Flight* **2**(50), 1006–1007 (1910).
3. R. L. Page, "Brief History of Flight Simulation," *SimTecT 2000 Proceedings* (John Wiley & Sons, Chichester, UK, 2000) pp. 11–17.
4. D. Allerton, *Principles of Flight Simulation* (John Wiley & Sons, Chichester, UK, 2009).
5. S. Casas, R. Olanda and N. Dey, "Motion cueing algorithms: A review: algorithms, evaluation and tuning," *Int. J. Virtual Augmented Reality* **1**(1), 90–106 (2017).
6. S. Nordmark, "Driving Simulators, Trends And Experiences," *Proceedings of the Driving Simulation Conference*, Paris, France (1994).
7. F. Colombet, M. Dagdelen, G. Reymond, C. Pere, F. Merienne and A. Kemeny, "Motion Cueing: What is the Impact on the Driver's Behavior," *Proceedings of the Driving Simulation Conference*, Paris, France (2008) pp. 171–181.
8. J. Challen, "Reality Bytes," *Driving Simulators* (2008) pp. 50–53.
9. J. Amend, N. Cheng, S. Fakhouri and B. Culley, "Soft robotics commercialization: Jamming grippers from research to product," *Soft. Rob.* **3**(4), 213–222 (2016).
10. S. Sadeghian Borojeni, S. C. Boll, W. Heuten, H. H. Bülthoff and L. Chuang, "Feel the Movement: Real Motion Influences Responses to Take-Over Requests in Highly Automated Vehicles," *Proceedings of the 2018 CHI Conference on Human Factors in Computing Systems*, Montreal, QC, Canada (ACM, 2018) p. 246.
11. H. Teufel, H.-G. Nusseck, K. Beykirch, J. Butler, M. Kerger and H. Bülthoff, "MPI Motion Simulator: Development and Analysis of a Novel Motion Simulator," *AIAA Modeling and Simulation Technologies Conference and Exhibit*, Hilton Head, South Carolina (2007) p. 6476.
12. J.-P. Merlet, *Parallel Robots* (Springer Science & Business Media, Berlin, 2006).
13. B. Dasgupta and T. Mruthyunjaya, "The Stewart platform manipulator: A review," *Mech. Mach. Theory* **35**(1), 15–40 (2000).
14. M. J. Tajaril, S. Pedrammehr, M. R. C. Qazani and M. J. Nategh, "The Effects of Joint Clearance on the Kinematic Error of the Hexapod Tables," *2017 5th RSI International Conference on Robotics and Mechatronics (ICRoM)*, Tehran, Iran (IEEE, 2017) pp. 39–44.
15. S. Pedrammehr, M. R. C. Qazani, H. Asadi and S. Nahavandi, "Control System Development of a Hexarotbased High-G Centrifugal Simulator," *20th IEEE International Conference on Industrial Technology IEEE-ICIT 2019*, Melbourne, Australia (2019).
16. S. Pedrammehr, M. R. C. Qazani, H. Asadi and S. Nahavandi, "Kinematic Manipulability Analysis of Hexarot Simulators," *20th IEEE International Conference on Industrial Technology, IEEE-ICIT 2019*, Melbourne, Australia (2019) pp. 13–15.

https://doi.org/10.1017/S0263574719001516 Published online by Cambridge University Press

17. S. Pedrammehr, M. R. C. Qazani, H. Abdi and S. Nahavandi, "Mathematical modelling of linear motion error for Hexarot parallel manipulators," *Appl. Math. Modell.* **40**(2), 942–954 (2016).
18. M. R. C. Qazani, S. Pedrammehr and M. J. Nategh, "A study on motion of machine tools' hexapod table on freeform surfaces with circular interpolation," *Int. J. Adv. Manuf. Technol.* **75**(9–12), 1763–1771 (2014).
19. M. R. C. Qazani, S. Pedrammehr, A. Rahmani, B. Danaei, M. M. Ettefagh, A. K. S. Rajab and H. Abdi "Kinematic analysis and workspace determination of hexarot-a novel 6-DOF parallel manipulator with a rotation-symmetric arm system," *Robotica* **33**(8), 1686–1703 (2015).
20. L. Johannesson, V. Berbyuk and T. Brogårdh, "Gantry-Tau–A New Three Degrees of Freedom Parallel Kinematic Robot," *Proceedings of the Mekatronikmöte 2003*, Göteborg, Sweden (2003) pp. 1–6.
21. I. Tyapin, G. Hovland and T. Brogardh, "Workspace optimisation of a reconfigurable parallel kinematic manipulator," *2007 IEEE/ASME International Conference on Advanced Intelligent Mechatronics*, Switzerland (IEEE, 2007) pp. 1–6.
22. I. Williams, G. Hovland and T. Brogardh, "Kinematic Error Calibration of the Gantry-Tau Parallel Manipulator," *Proceedings 2006 IEEE International Conference on Robotics and Automation*, Orlando, Florida (IEEE, 2006), pp. 4199–4204.
23. M. Murray, G. Hovland and T. Brogårdh, "Singularityfree Reconfiguration of the 5-DOF Gantry-Tau Parallel Kinematic Machine," *Proceedings of 2nd International Workshop on Fundamental Issues and Future Research Directions for Parallel Mechanisms and Manipulators*, Citeseer, Montpellier (2008) pp. 21–22.
24. I. Dressler, "Modeling and Control of Stiff Robots for Flexible Manufacturing," *Ph.D. Thesis* (2012).
25. M. A. Khosravi and H. D. Taghirad, "Dynamic modeling and control of parallel robots with elastic cables: Singular perturbation approach," *IEEE Trans. Rob.* **30**(3), 694–704 (2014).
26. H. S. Kim, Y. M. Cho and K.-I. Lee, "Robust nonlinear task space control for 6 DOF parallel manipulator," *Automatica* **41**(9), 1591–1600 (2005).
27. E. Mamdani and N. Baaklini, "Prescriptive method for deriving control policy in a fuzzy-logic controller," *Electron. Lett.* **11**(25), 625–626 (1975).
28. G. K. Mann, B.-G. Hu and R. G. Gosine, "Two-level tuning of fuzzy PID controllers," *IEEE Trans. Syst. Man Cybern. Part B* **31**(2), 263–269 (2001).
29. H. Asadi, S. Kaboli, M. Oladazimi and M. Safari, "A review on Li-ion battery charger techniques and optimize battery charger performance by fuzzy logic," *ICICA* **18**(201), 89–96 (2011).
30. H. Asadi, S. Mohamed and S. Nahavandi, "Incorporating human perception with the motion washout filter using fuzzy logic control," *IEEE/ASME Trans. Mech.* **20**(6), 3276–3284 (2015).
31. H. Asadi, A. Mohammadi, S. Mohamed, D. R. Zadeh and S. Nahavandi, "Adaptive Washout Algorithm based Fuzzy Tuning for Improving Human Perception," *International Conference on Neural Information Processing* (Springer, Berlin, 2014) pp. 483–492.
32. H. Asadi, C. P. Lim, S. Mohamed, D. Nahavandi and S. Nahavandi, "Increasing motion fidelity in driving simulators using a fuzzy-based washout filter," *IEEE Trans. Intell. Veh.* **4**(2), 298–308 (2019).
33. H. Asadi, C. P. Lim, A. Mohammadi, S. Mohamed, S. Nahavandi and L. Shanmugam, "A genetic algorithm–based nonlinear scaling method for optimal motion cueing algorithm in driving simulator," *Proc. Inst. Mech. Eng. Part I: J. Syst. Cont. Eng.* **232**(8), 1025–1038 (2018).
34. H. Asadi, S. Mohamed, K. Nelson, S. Nahavandi and M. Oladazimi, "An Optimal Washout Filter based on Genetic Algorithm Compensators for Improving Simulator Driver Perception," *DSC 2015: Proceedings of the Driving Simulation Conference & Exhibition* (Max Planck Institute for the Advancement of Science, Germany, 2015) pp. 1–10.
35. H. Asadi, S. Mohamed, K. Nelson, S. Nahavandi and D. R. Zadeh, "Human Perception-based Washout Filtering using Genetic Algorithm," *International Conference on Neural Information Processing* (Springer, Berlin, 2015) pp. 401–411.
36. M. Dagdelen, G. Reymond, A. Kemeny, M. Bordier and N. Maïki, "MPC based Motion Cueing Algorithm: Development and Application to the ULTIMATE Driving Simulator," *Conférence Simulation de Conduite*, Paris (2004) pp. 221–233.
37. E. Groen and W. Bles, "How to use body tilt for the simulation of linear self motion," *J. Vestibular Res.* **14**(5), 375–385 (2004).
38. N. J. Garrett and M. C. Best, "Model predictive driving simulator motion cueing algorithm with actuator-based constraints," *Veh. Sys. Dyn.* **51**(8), 1151–1172 (2013).
39. A. Mohammadi, H. Asadi, S. Mohamed, K. Nelson and S. Nahavandi, "MPC-based Motion Cueing Algorithm with Short Prediction Horizon using Exponential Weighting," *2016 IEEE International Conference on Systems, Man, and Cybernetics (SMC)*, Budapest (IEEE, 2016) pp. 000521–000526.
40. A. Mohammadi, S. H. Asadi, K. Nelson and S. Nahavandi, "Future Reference Prediction in Model Predictive Control Based Driving Simulators," *Australasian Conference on Robotics and Automation (ACRA2016)*, Brisbane, Australia (2016).
41. A. Mohammadi, H. Asadi, S. Mohamed, K. Nelson and S. Nahavandi, "Optimizing model predictive control horizons using genetic algorithm for motion cueing algorithm," *Expert Syst. Appl.* **92**, 73–81 (2018).
42. A. Mohammadi, H. Asadi, S. Mohamed, K. Nelson and S. Nahavandi, "Multiobjective and interactive genetic algorithms for weight tuning of a model predictive control-based motion cueing algorithm," *IEEE Trans. Cybern.* **49**(9), 3471–3481 (2018).
43. M. R. C. Qazani, H. Asadi and S. Nahavandi, "A Decoupled Linear Model Predictive Control-Based Motion Cueing Algorithm for simulation-based motion platform with limited workspace," *IEEE International Conference on Systems, Man, and Cybernetics (SMC)*, Bari, Italy (2019) pp. 1–6.

44. M. R. C. Qazani, H. Asadi and S. Nahavandi, "A Model Predictive Control-Based Motion Cueing Algorithm with Consideration of Joints' Limitations for Hexapod Motion Platform," *SMC*, Bari, Italy (IEEE, 2019).
45. I. Dressler, A. Robertsson and R. Johansson, "Accuracy of Kinematic and Dynamic Models of a Gantry-Tau Parallel Kinematic Robot," *Proceedings 2007 IEEE International Conference on Robotics and Automation*, Roma, Italy (IEEE, 2007) pp. 883–888.
46. M. R. C. Qazani, S. Pedrammehr, A. Rahmani, M. Shahryari, A. K. S. Rajab and M. M. Ettefagh, "An experimental study on motion error of hexarot parallel manipulator," *Int. J. Adv. Manuf. Technol.* **72**(9–12), pp. 1361–1376 (2014).
47. S. Pedrammehr, M. R. C. Qazani and S. Nahavandi, "A Novel Axis Symmetric Parallel Mechanism with Coaxial Actuated Arms," *2018 4th International Conference on Control, Automation and Robotics (ICCAR)*, Auckland, New Zealand (IEEE, 2018) pp. 476–480.
48. S. Pedrammehr, M. R. C. Qazani, S. Nahavandi and H. Asadi, "Control System Development of a Hexarot-based High-G Centrifugal Simulator," *Presented at the The 20th IEEE International Conference on Industrial Technology*, Melbourne, Australia (2019).
49. M. Mitchell, *An Introduction to Genetic Algorithms* (MIT Press, Cambridge, MA, USA, 1998).
50. J. Sadeghi, S. Sadeghi and S. T. A. Niaki, "Optimizing a hybrid vendor-managed inventory and transportation problem with fuzzy demand: An improved particle swarm optimization algorithm," *Inf. Sci.* **272**, 126–144 (2014).
51. L. A. Zadeh, *Fuzzy Logic: Advanced Concepts and Structures* (IEEE Educational Activities Department, MIT Press, Cambridge, Massachusetts, USA, 1992).
52. W.-Y. Lin, W.-Y. Lee and T.-P. Hong, "Adapting crossover and mutation rates in genetic algorithms," *J. Inf. Sci. Eng.* **19**(5), 889–903 (2003).
53. K. Deb and S. Agrawal, "Understanding Interactions among Genetic Algorithm Parameters," **In:** *FOGA* (Morgan Kaufmann, San Francisco, CA, USA, 1998) pp. 265–286.
54. K. De Jong, "Adaptive system design: A genetic approach," *IEEE Trans. Syst. Man Cybern.* **10**(9), 566–574 (1980).
55. K. A. De Jong, "Analysis of the behavior of a class of genetic adaptive systems," PhD dissertation (University of Michigan Press, Ann Arbor, MI, USA, 1975).
56. J. Hesser and R. Männer, "Towards an Optimal Mutation Probability for Genetic Algorithms," *International Conference on Parallel Problem Solving from Nature* (Springer, Berlin, 1990) pp. 23–32.
57. G. Ochoa, I. Harvey and H. Buxton, "On Recombination and Optimal Mutation Rates," *Proceedings of the 1st Annual Conference on Genetic and Evolutionary Computation-Volume 1* (Morgan Kaufmann Publishers Inc., San Francisco, CA, USA, 1999) pp. 488–495.
58. O. Roeva, S. Fidanova and M. Paprzycki, "Population Size Influence on the Genetic and Ant Algorithms Performance in Case of Cultivation Process Modeling," *2013 Federated Conference on Computer Science and Information Systems (FedCSIS)*, Krakow, Poland (2015) pp. 107–120.
59. H. Asadi, S. Mohamed, C. P. Lim and S. Nahavandi, "A review on otolith models in human perception," *Behav. Brain Res.* **309**, 67–76 (2016).
60. J. A. Houck, R. J. Telban and F. M. Cardullo, "Motion cueing algorithm development: Human-centered linear and nonlinear approaches," (NASA, Hampton, 2005). Available from: https://archive.org/details/NASA_NTRS_Archive_20050180246
61. H. Asadi, S. Mohamed, C. P. Lim, S. Nahavandi and E. Nalivaiko, "Semicircular canal modeling in human perception," *Rev. Neurosci.* **28**(5), 537–549 (2017).
62. H. Asadi, S. Mohamed, D. Rahim Zadeh and S. Nahavandi, "Optimisation of nonlinear motion cueing algorithm based on genetic algorithm," *Veh. Syst. Dyn.* **53**(4), 526–545 (2015).
63. M. R. C. Qazani, H. Asadi, S. Pedrammehr and S. Nahavandi, "Performance Analysis and Dexterity Monitoring of Hexapod-Based Simulator," *2018 4th International Conference on Control, Automation and Robotics (ICCAR)*, Auckland, New Zealand (IEEE, 2018) pp. 226–231.
64. coin-or, *qpOASES*, https://projects.coin-or.org/qpOASES.
65. S. Pedrammehr, M. R. C. Qazani, H. Asadi and S. Nahavandi, "Kinematic Manipulability Analysis of Hexarot Simulators," *20th IEEE International Conference on Industrial Technology*, Melbourne, Australia (2019).
66. R. A. Fisher, "Statistical methods for research workers," **In:** *Breakthroughs in Statistics* (Springer, Berlin, 1992) pp. 66–70.
67. M. G. Kendall and A. Stuart, "The advanced theory of statistics," (Charles Griffin & Company Limited, London, UK, 1945).
68. W. H. Press, S. A. Teukolsky, W. T. Vetterling and B. P. Flannery, *Numerical Recipes in C++: The Art of Scientific Computing*, vol. 2 (Cambridge University Press, Cambridge, 2007) p. 1002.
69. S. Moro, P. Ramos, J. Esmerado and S. M. J. Jalali, "Can we trace back hotel online reviews' characteristics using gamification features?" *Int. J. Inf. Manage.* **44**, 88–95 (2019).
70. S. M. J. Jalali, E. Mahdizadeh, M. R. Mahmoudi and S. Moro, "Analytical assessment process of e-learning domain research between 1980 and 2014," *Int. J. Manage. Educ.* **12**(1), 43–56 (2018).
71. J. Jalali, S. Mohammad and H. W. Park, "Conversations about open data on Twitter," *IJCT* **13**(1), 31–37 (2017).
72. H. Zheng, J. Zhang and S. Nahavandi, "Learning to detect texture objects by artificial immune approaches," *Future Gener. Comput. Syst.* **20**(7), 1197–1208 (2004).

73. M. J. Amiri, J. Abedi-Koupai, S. M. Jafar Jalali and S. F. Mousavi, "Modeling of fixed-bed column system of Hg (II) ions on ostrich bone ash/nZVI composite by artificial neural network," *J. Environ. Eng.* **143**(9), 04017061 (2017).
74. S. M. J. Jalali, A. Khosravi, R. Alizadehsani, S. M. Salaken, P. M. Kebria, R. Puri and S. Nahavandi, "Parsimonious Evolutionary-based Model Development for Detecting Artery Disease," *20th IEEE International Conference on Industrial Technology*, Melbourne, Australia (2019) pp. 800–805.
75. M. Oladazimi, F. M. Vaneghi, M. Safari, H. Asadi and S. H. A. Kaboli, "A Review for Feature Extraction of EMG Signal Processing," *4th International Conference on Computer and Automation Engineering (ICCAE 2012)*, Mumbai, India (ASME Press, 2012).
76. S. Jalali, S. Moro, M. R. Mahmoudi, K. A. Ghaffary, M. Maleki and A. Alidoostan, "A comparative analysis of classifiers in cancer prediction using multiple data mining techniques," *Comp. Anal. Classifiers Cancer Prediction Multiple Data Min. Tech.* **1**(2), 166–178 (2017).
77. I. R. Vanani and S. M. J. Jalali, "A comparative analysis of emerging scientific themes in business analytics," *Int. J. Bus. Inf. Syst.* **29**(2), 183–206 (2018).
78. S. M. J. Jalali and H. W. Park, "State of the art in business analytics: Themes and collaborations," *Qual. Quant.* **52**(2), 627–633 (2018).
79. I. R. Vanani and S. M. J. Jalali, "Analytical evaluation of emerging scientific trends in business intelligence through the utilisation of burst detection algorithm," *Int. J. Bibliometr. Bus. Manage.* **1**(1), 70–79 (2017).
80. S. M. J. Jalali and E. Mahizadeh, "The investigation of e-business trends by using social network analysis technique during 1980–2015," *J. Inf. Tech. Manage.* **8**(3), 499–518 (2016).
81. A. Mohammadi, H. Asadi, S. Mohamed, K. Nelson and S. Nahavandi, "openGA, a C++ Genetic Algorithm Library," *2017 IEEE International Conference on Systems, Man, and Cybernetics (SMC)*, Banff, Canada (IEEE, 2017) pp. 2051–2056.

Appendix

The geometric parameters of the Gantry-Tau-3R manipulator:

The length of the guideways:

$$l_1, l_2, l_3 = 3000 \text{ (mm)};$$

The length of the links:

$$\left|L_{1-3,1-3}\right| = 3000 \text{ (mm)}; \; |L_4| = 100 \text{ (mm)}; \; |L_5| = 285 \text{ (mm)}; \; |L_6| = 337 \text{ (mm)};$$

The start position of the guideways, A_i^s (mm):

$$A_1^s = \begin{bmatrix} 0 & -1250 & 1250 \end{bmatrix}^T; \; A_2^s = \begin{bmatrix} 0 & 1250 & 1250 \end{bmatrix}^T; \; A_3^s = \begin{bmatrix} 0 & -1250 & -1250 \end{bmatrix}^T$$

The joint position of the carts, $C_{i,k}$ (mm):

$$C_{1,1} = \begin{bmatrix} 0 & 0 & 0 \end{bmatrix}^T; \; C_{2,1} = \begin{bmatrix} 0 & 143 & 0 \end{bmatrix}^T; \; C_{2,2} = \begin{bmatrix} -124 & 0 & 0 \end{bmatrix}^T; \; C_{3,1} = \begin{bmatrix} 0 & 143 & 0 \end{bmatrix}^T;$$
$$C_{3,2} = \begin{bmatrix} -124 & -72 & 0 \end{bmatrix}^T; \; C_{3,3} = \begin{bmatrix} 124 & -72 & 0 \end{bmatrix}^T$$

The joint position of the platform, $D_{i,k}$ (mm):

$$D_{1,1} = \begin{bmatrix} 0 & 127.01 & 0 \end{bmatrix}^T; \; D_{2,1} = \begin{bmatrix} 0 & -124.99 & 59.81 \end{bmatrix}^T; \; D_{2,2} = \begin{bmatrix} 0 & 127.01 & 0 \end{bmatrix}^T;$$
$$D_{3,1} = \begin{bmatrix} 143.45 & 1.01 & 99.81 \end{bmatrix}^T; \; D_{3,2} = \begin{bmatrix} 0 & -124.99 & -90.19 \end{bmatrix}^T; \; D_{3,3} = \begin{bmatrix} 0 & 127.01 & -90.19 \end{bmatrix}^T$$

https://doi.org/10.1017/S0263574719001516 Published online by Cambridge University Press